Alexandre LÊ
alexandre-thanh.le@safrangroup.com

Sorbonne Université, Paris Université
Safran Electronics & Defense, Inria Paris, CNRS

November 3, 2022

On the Certification of the Kinematics of 3-DOF Spherical Parallel Manipulators

A Contributed Talk in Algorithms and Software

Maple Conference 2022

Overview

Spherical Parallel Manipulators: Context and Challenges

About me

- Alexandre LÊ, PhD Student (CIFRE)
- Academic supervisors: Fabrice ROUILLIER (Inria – Sorbonne Université), Damien CHABLAT (CNRS – Centrale Nantes). Industrial: Guillaume RANCE (Safran Electronics & Defense)

About me

- Alexandre Lê, PhD Student (CIFRE)
- Academic supervisors: Fabrice Rouillier (Inria – Sorbonne Université), Damien Chablat (CNRS – Centrale Nantes). Industrial: Guillaume Rance (Safran Electronics & Defense)

Problem statement

- Use a *parallel robot* to take a *panorama* picture on a *stabilized* moving career with high definition cameras

About me

- Alexandre Lê, PhD Student (CIFRE)
- Academic supervisors: Fabrice Rouillier (Inria – Sorbonne Université), Damien Chablat (CNRS – Centrale Nantes). Industrial: Guillaume Rance (Safran Electronics & Defense)

Problem statement

- Use a *parallel robot* to take a *panorama* picture on a *stabilized* moving career with high definition cameras
- Idea of mechanism: 3-DOF **Spherical Parallel Manipulator** ([Gosselin and Hamel, 1994]) with coaxial input shafts ([Tursynbek and Shintemirov, 2020])

What is a parallel robot?

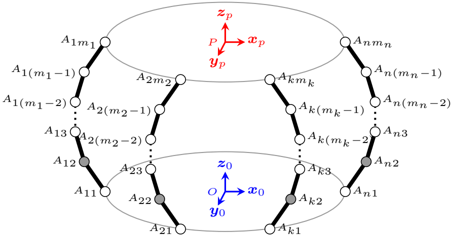

(a) General structure of a parallel robot

(b) Example of a parallel robot

Figure: Parallel robots: definition and examples

What is a parallel robot?

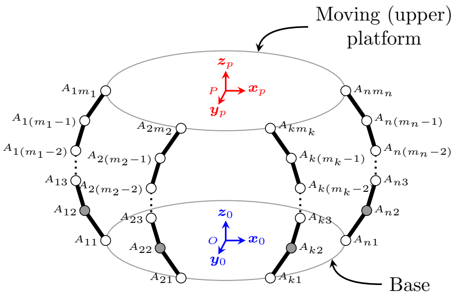

(a) General structure of a parallel robot

(b) Example of a parallel robot

Figure: Parallel robots: definition and examples

What is a parallel robot?

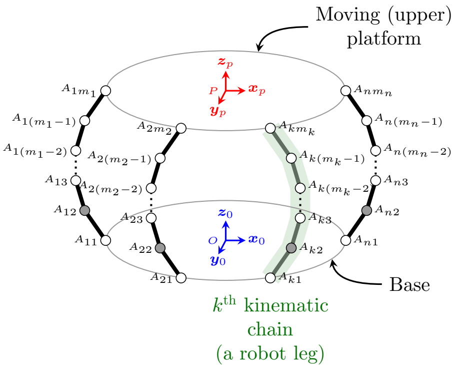

(a) General structure of a parallel robot

(b) Example of a parallel robot

Figure: Parallel robots: definition and examples

What is a parallel robot?

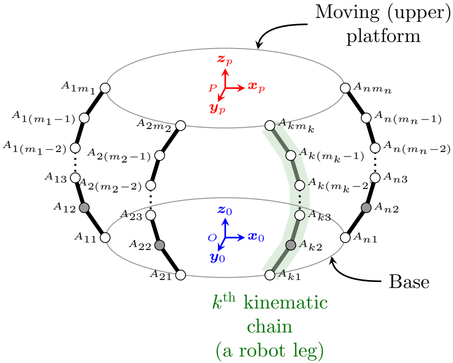

(a) General structure of a parallel robot

(b) Example of a parallel robot

Figure: Parallel robots: definition and examples

What is a parallel robot?

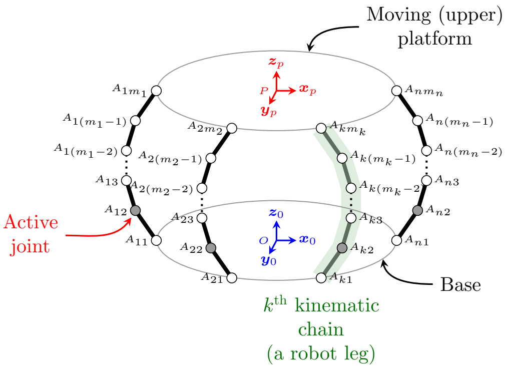

(a) General structure of a parallel robot

(b) Example of a parallel robot

Figure: Parallel robots: definition and examples

What is a parallel robot?

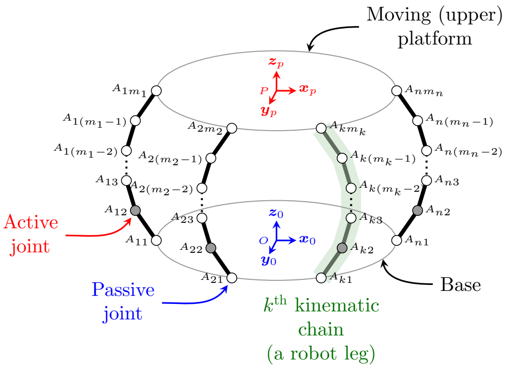

(a) General structure of a parallel robot

(b) Example of a parallel robot

Figure: Parallel robots: definition and examples

What is a parallel robot?

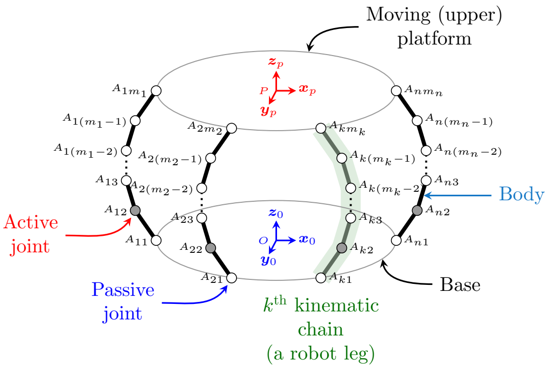

(a) General structure of a parallel robot

(b) Example of a parallel robot

Figure: Parallel robots: definition and examples

What is a parallel robot?

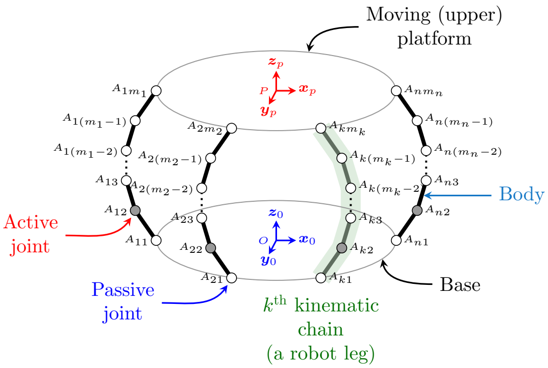

(a) General structure of a parallel robot

(b) Example of a parallel robot

Figure: Parallel robots: definition and examples

- Current example: Hexapod from Symétrie (commercial device)

What is a parallel robot?

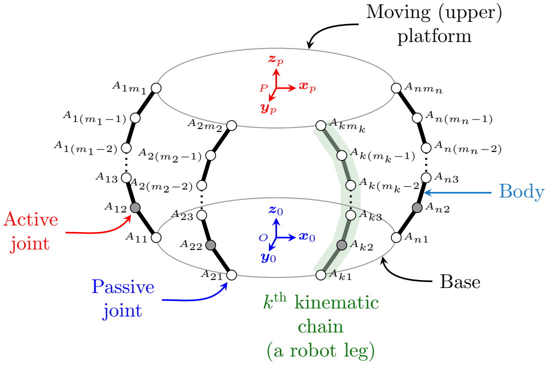

(a) General structure of a parallel robot

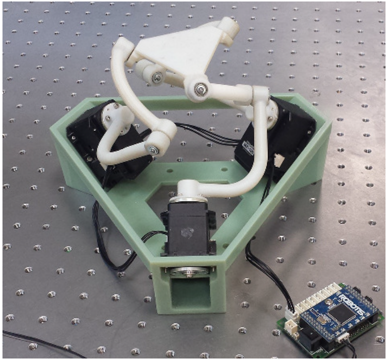

(b) Example of a parallel robot

Figure: Parallel robots: definition and examples

- Current example: "Agile wrist" of [Shintemirov et al., 2015] (prototype)

What is a parallel robot?

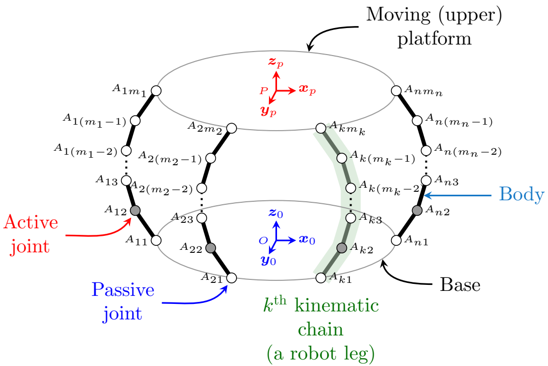

(a) General structure of a parallel robot

(b) Example of a parallel robot

Figure: Parallel robots: definition and examples

- Current example: “Coaxial agile wrist” of [Tursynbek et al., 2019] (prototype)

Modeling of a 3-DOF non-redundant SPM

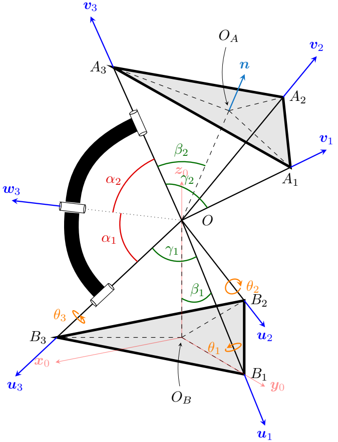

Figure: A general SPM

- 3 actuators $\boldsymbol{\theta} \triangleq \begin{bmatrix} \theta_1 & \theta_2 & \theta_3 \end{bmatrix}^\mathsf{T}$
- 3 DOF in orientation $\boldsymbol{\chi} \triangleq \begin{bmatrix} \chi_1 & \chi_2 & \chi_3 \end{bmatrix}^\mathsf{T}$
- Rotation sequence: $\boldsymbol{M} \triangleq \boldsymbol{R}_z(\chi_3)\boldsymbol{R}_x(\chi_1)\boldsymbol{R}_y(\chi_2)$
- $\boldsymbol{\varpi} \triangleq \begin{bmatrix} \alpha_1 & \alpha_2 & \beta_1 & \beta_2 & \eta_1 & \eta_2 & \eta_3 \end{bmatrix}^\mathsf{T}$ are the *conception parameters*

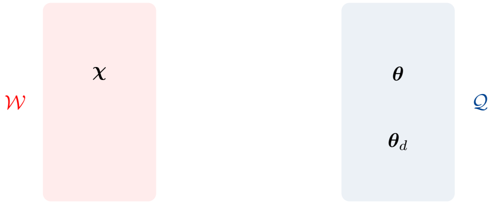

Figure: Principle of the geometric model

Modeling of a 3-DOF non-redundant SPM

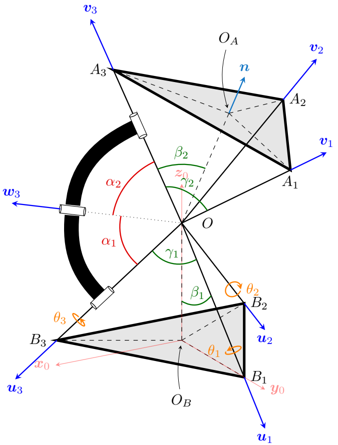

Figure: A general SPM

- 3 actuators $\boldsymbol{\theta} \triangleq \begin{bmatrix} \theta_1 & \theta_2 & \theta_3 \end{bmatrix}^\mathsf{T}$
- 3 DOF in orientation $\boldsymbol{\chi} \triangleq \begin{bmatrix} \chi_1 & \chi_2 & \chi_3 \end{bmatrix}^\mathsf{T}$
- Rotation sequence: $\boldsymbol{M} \triangleq \boldsymbol{R}_z(\chi_3)\boldsymbol{R}_x(\chi_1)\boldsymbol{R}_y(\chi_2)$
- $\boldsymbol{\varpi} \triangleq \begin{bmatrix} \alpha_1 & \alpha_2 & \beta_1 & \beta_2 & \eta_1 & \eta_2 & \eta_3 \end{bmatrix}^\mathsf{T}$ are the *conception parameters*

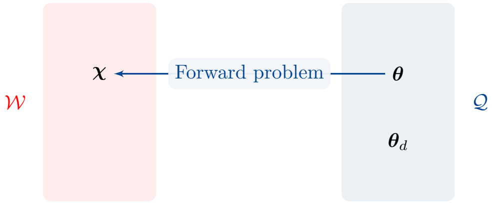

Figure: Principle of the geometric model

Modeling of a 3-DOF non-redundant SPM

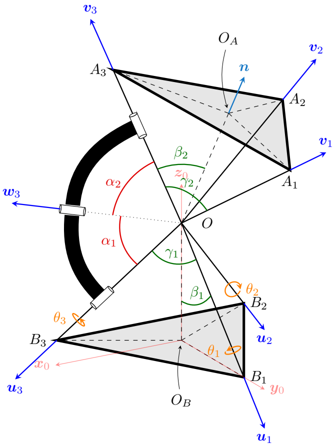

Figure: A general SPM

- 3 actuators $\boldsymbol{\theta} \triangleq \begin{bmatrix} \theta_1 & \theta_2 & \theta_3 \end{bmatrix}^\mathsf{T}$
- 3 DOF in orientation $\boldsymbol{\chi} \triangleq \begin{bmatrix} \chi_1 & \chi_2 & \chi_3 \end{bmatrix}^\mathsf{T}$
- Rotation sequence: $\boldsymbol{M} \triangleq \boldsymbol{R}_z(\chi_3)\boldsymbol{R}_x(\chi_1)\boldsymbol{R}_y(\chi_2)$
- $\boldsymbol{\varpi} \triangleq \begin{bmatrix} \alpha_1 & \alpha_2 & \beta_1 & \beta_2 & \eta_1 & \eta_2 & \eta_3 \end{bmatrix}^\mathsf{T}$ are the *conception parameters*

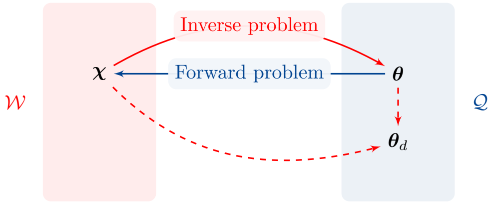

Figure: Principle of the geometric model

Modeling of a 3-DOF non-redundant SPM

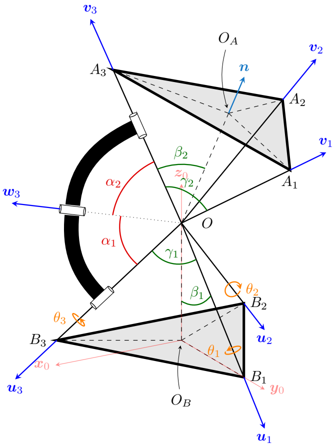

Figure: A general SPM

- 3 actuators $\boldsymbol{\theta} \triangleq \begin{bmatrix} \theta_1 & \theta_2 & \theta_3 \end{bmatrix}^\mathsf{T}$
- 3 DOF in orientation $\boldsymbol{\chi} \triangleq \begin{bmatrix} \chi_1 & \chi_2 & \chi_3 \end{bmatrix}^\mathsf{T}$
- Rotation sequence: $\boldsymbol{M} \triangleq \boldsymbol{R}_z(\chi_3)\boldsymbol{R}_x(\chi_1)\boldsymbol{R}_y(\chi_2)$
- $\boldsymbol{\varpi} \triangleq \begin{bmatrix} \alpha_1 & \alpha_2 & \beta_1 & \beta_2 & \eta_1 & \eta_2 & \eta_3 \end{bmatrix}^\mathsf{T}$ are the *conception parameters*

Geometric modeling of 3-DOF SPMs

$$\boldsymbol{f}\left(\boldsymbol{\theta},\boldsymbol{\chi}\right) \triangleq \begin{bmatrix} \boldsymbol{w}_1^\mathsf{T}(\theta_1,\boldsymbol{\varpi})\,\boldsymbol{v}_1(\chi_1,\chi_2,\chi_3,\boldsymbol{\varpi}) - \cos\left(\alpha_2\right) \\ \boldsymbol{w}_2^\mathsf{T}(\theta_2,\boldsymbol{\varpi})\,\boldsymbol{v}_2(\chi_1,\chi_2,\chi_3,\boldsymbol{\varpi}) - \cos\left(\alpha_2\right) \\ \boldsymbol{w}_3^\mathsf{T}(\theta_3,\boldsymbol{\varpi})\,\boldsymbol{v}_3(\chi_1,\chi_2,\chi_3,\boldsymbol{\varpi}) - \cos\left(\alpha_2\right) \end{bmatrix} = \boldsymbol{0}$$

- Non-linear equations

Modeling of a 3-DOF non-redundant SPM

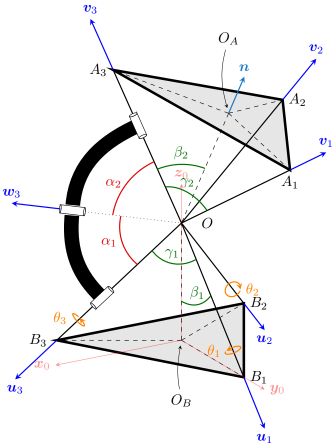

Figure: A general SPM

- 3 actuators $\boldsymbol{\theta} \triangleq \begin{bmatrix} \theta_1 & \theta_2 & \theta_3 \end{bmatrix}^\mathsf{T}$
- 3 DOF in orientation $\boldsymbol{\chi} \triangleq \begin{bmatrix} \chi_1 & \chi_2 & \chi_3 \end{bmatrix}^\mathsf{T}$
- Rotation sequence: $\boldsymbol{M} \triangleq \boldsymbol{R}_z(\chi_3)\boldsymbol{R}_x(\chi_1)\boldsymbol{R}_y(\chi_2)$
- $\boldsymbol{\varpi} \triangleq \begin{bmatrix} \alpha_1 & \alpha_2 & \beta_1 & \beta_2 & \eta_1 & \eta_2 & \eta_3 \end{bmatrix}^\mathsf{T}$ are the *conception parameters*

Geometric modeling of 3-DOF SPMs

$$\boldsymbol{f}(\boldsymbol{\theta}, \boldsymbol{\chi}) \xrightarrow[\substack{o_i \triangleq \tan\left(\frac{\chi_i}{2}\right) \\ j_i \triangleq \tan\left(\frac{\theta_i}{2}\right)}]{\text{to polynomials}} \boldsymbol{S} \triangleq \begin{cases} p_1(j_1, o_1, o_2, o_3, \boldsymbol{\varpi}) = 0 \\ p_2(j_2, o_1, o_2, o_3, \boldsymbol{\varpi}) = 0 \\ p_3(j_3, o_1, o_2, o_3, \boldsymbol{\varpi}) = 0 \end{cases}$$

- $\boldsymbol{S}$ is *generically zero-dimensional* and is associated with $\mathcal{V}(\mathcal{I}) = \mathcal{V}(\langle p_1, p_2, p_3 \rangle)$

Special case: SPM with coaxial input shafts

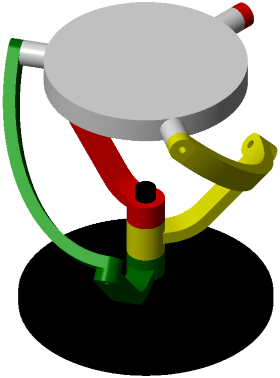

Figure: SPM with coaxial input shafts

Parameter	Values (rad)	Details
η_1	0	
η_2	$2\pi/3$	
η_3	$4\pi/3$	
α_1	$\pi/4$	proximal link
α_2	$\pi/2$	distal link
β_1	0	coaxial input shafts
β_2	$\pi/2$	

Table: Exact values of the conception parameters

- Kinematics: optimal design [Bai, 2010]
- Coaxiality: unlimited rolling
- Specifications: stabilizing pitch and roll $\pm 20°$

$$\mathcal{W}^\star \triangleq \{\boldsymbol{\chi} \in \mathbb{R}^3 \text{ s.t. } |\chi_i| \leq 20°,\ \forall i \in [\![1,2]\!]\}$$

Pathological configurations

- Loss of at least 1 DOF: Type-1 singularity
- Gain of at least 1 **uncontrollable** DOF: Type-2 singularity ▷ Example (PAMINSA – S. Briot)

Pathological configurations

- Loss of at least 1 DOF: Type-1 singularity
- Gain of at least 1 **uncontrollable** DOF: Type-2 singularity ▷ Example (PAMINSA – S. BRIOT)

Challenges

- Non-linearities, modeling
- Uncertainties (numerical, physical) and Numerical instabilities

Parallel robots: what could go wrong?

Pathological configurations

- Loss of at least 1 DOF: Type-1 singularity
- Gain of at least 1 **uncontrollable** DOF: Type-2 singularity ▷ Example (PAMINSA – S. Briot)

Challenges

- Non-linearities, modeling
- Uncertainties (numerical, physical) and Numerical instabilities

The goal

Ensure *the absence of singularities in our prescribed workspace* $\mathcal{W}^\star$ *for our application* ***despite uncertainties****.*

Parallel robots: what could go wrong?

Pathological configurations

- Loss of at least 1 DOF: Type-1 singularity
- Gain of at least 1 **uncontrollable** DOF: Type-2 singularity ▷ Example (PAMINSA – S. Briot)

Challenges

- Non-linearities, modeling
- Uncertainties (numerical, physical) and Numerical instabilities

The goal

*Certify a (spherical parallel) mechanism **given specifications in** $\mathcal{W}^{\star}$.*

Certification of the IGM (Inverse Kinematics)

Discriminant variety (DV)

Definition (Discriminant Variety [Lazard and Rouillier, 2007, Chablat et al., 2020])

The *minimal* discriminant variety of $\mathcal{V}(\mathcal{I})$ w.r.t. $\mathrm{proj}_{\boldsymbol{U}}$ denoted as $\mathcal{W}_D$ is the smallest algebraic variety of $\mathbb{C}^d$ such that given any simply connected subset $\mathcal{C}$ of $\mathbb{R}^d \setminus \mathcal{W}_D$, the number of real solutions of $\boldsymbol{S}$ is constant over $\boldsymbol{U}$. In our case,

$$\mathcal{W}_D \triangleq \mathcal{W}_{\mathrm{sd}} \cup \mathcal{W}_c \cup \mathcal{W}_\infty$$

where:

- $\mathcal{W}_{\mathrm{sd}}$ is the closure of the projection by $\mathrm{proj}_{\boldsymbol{U}}$ of the components of $\mathcal{V}(\mathcal{I})$ of dimension $< d$
- $\mathcal{W}_c$ is the union of the closure of the critical values of $\mathrm{proj}_{\boldsymbol{U}}$ in restriction to $\mathcal{V}(\mathcal{I})$ and of the projection of singular values of $\mathcal{V}(\mathcal{I})$
- $\mathcal{W}_\infty$ is the set of $\boldsymbol{U} = (U_1, \ldots, U_d)$ such that $\mathrm{proj}^{-1}(\mathcal{C}) \cap \mathcal{V}(\mathcal{I})$ is not compact for any compact neighborhood $\mathcal{C}$ of $\boldsymbol{U}$ in $\mathrm{proj}_{\boldsymbol{U}}(\mathcal{V}(\mathcal{I}))$.

DV of the Inverse Geometric Model: Computation

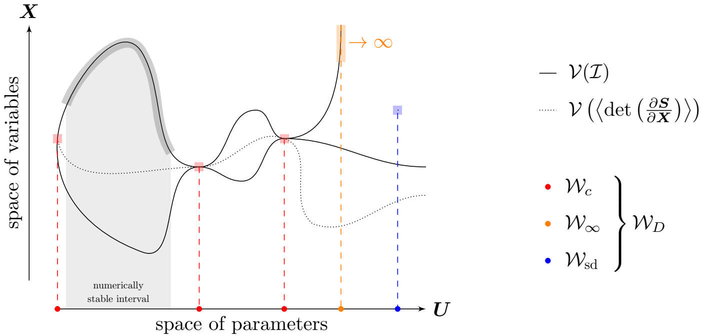

Figure: Certification by avoiding the discriminant variety $\mathcal{W}_D$ w.r.t. the projection onto the paramater space

- IGM:

DV of the Inverse Geometric Model: Computation

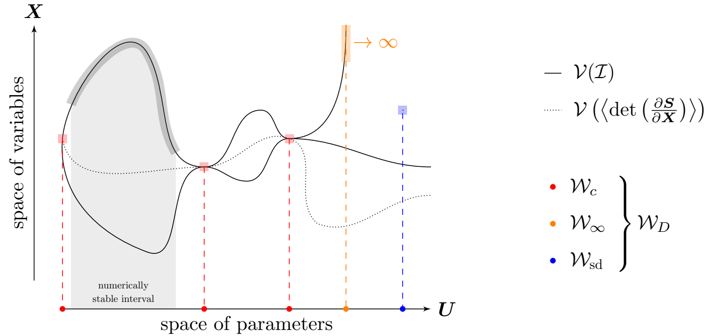

Figure: Certification by avoiding the discriminant variety $\mathcal{W}_D$ w.r.t. the projection onto the paramater space

- IGM: each polynomial p_i is univariate w.r.t. the unknown j_i, $\forall\, i \in [\![1, 3]\!]$

$$\mathcal{W}_D(o_1, o_2, o_3) = \bigcup_{i=1}^{n_a} \text{Res}\left(p_i, \frac{\partial p_i}{\partial j_i}, j_i\right) = \bigcup_{i=1}^{n_a} -\,\text{LC}\left(p_i, j_i\right)\,\text{discrim}\left(p_i, j_i\right) \qquad (1)$$

DV of the Inverse Geometric Model: Plots

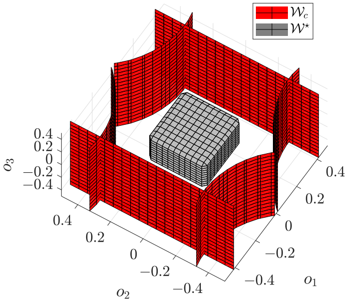

(a) Critical points of the IGM (Type-1 singularities)

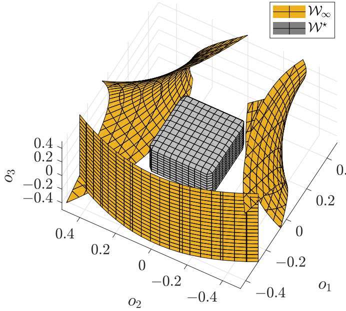

(b) "Infinite points" of the IGM

Figure: Discriminant variety of the IGM w.r.t. the projection onto the orientation space

DV of the Inverse Geometric Model: Plots

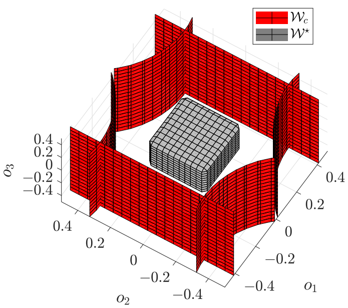

(a) Critical points of the IGM (Type-1 singularities)

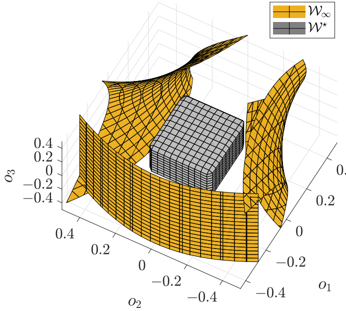

(b) “Infinite points” of the IGM

Figure: Discriminant variety of the IGM w.r.t. the projection onto the orientation space

- Type-1 singularities: invariant w.r.t. $o_3 \equiv \chi_3$ (yaw)

DV of the Inverse Geometric Model: Plots

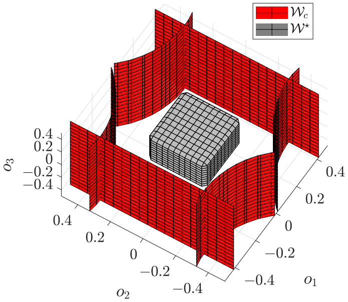

(a) Critical points of the IGM (Type-1 singularities)

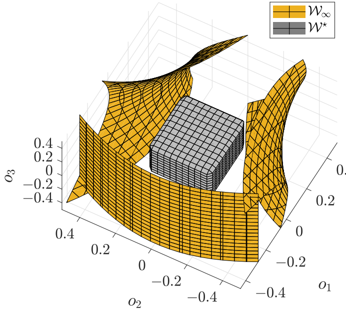

(b) “Infinite points” of the IGM

Figure: Discriminant variety of the IGM w.r.t. the projection onto the orientation space

- $\mathcal{W}^\star$ is Type-1 singular free

Type-1 singularities of the SPM

Physical interpretation

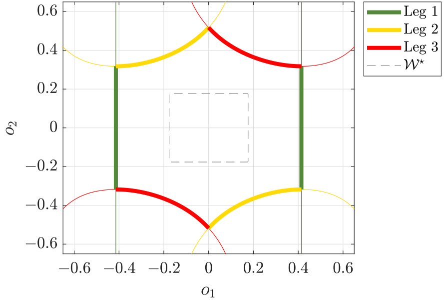

Figure: Type-1 singularity loci of the SPM in the orientation space

- Type-1 singularities:

Type-1 singularities of the SPM

Physical interpretation

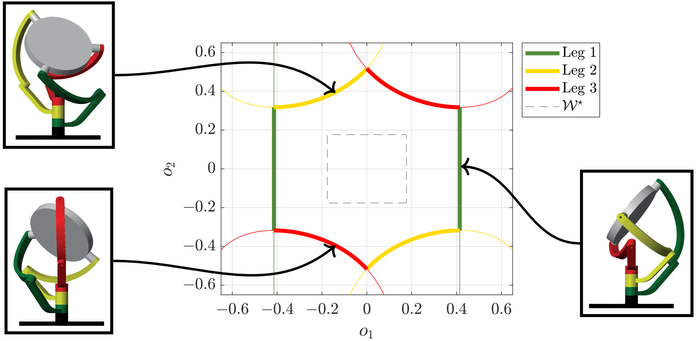

Figure: Type-1 singularity loci of the SPM in the orientation space

- Type-1 singularities: at least one leg being (un)folded

Computation of the joint stops

- Compute IGM($\mathcal{W}^\star$)

Computation of the joint stops

- Compute $\mathrm{IGM}(\mathcal{W}^\star) \triangleq \mathcal{Q}^\star$

Computation of the joint stops

- Compute $\mathrm{IGM}(\mathcal{W}^\star) \triangleq \mathcal{Q}^\star$ and set the *joint stops* $\mathcal{Q}_0^\star$

Computation of the joint stops

- Compute $\mathrm{IGM}(\mathcal{W}^\star) \triangleq \mathcal{Q}^\star$ and set the *joint stops* $\mathcal{Q}_0^\star$
- Interval analysis $\longrightarrow$ *Ball arithmetic* [Hoeven, 2010, Johansson, 2019]

- Compute $\mathrm{IGM}(\mathcal{W}^\star) \triangleq \mathcal{Q}^\star$ and set the *joint stops* $\mathcal{Q}_0^\star$
- Interval analysis $\longrightarrow$ *Ball arithmetic* [Hoeven, 2010, Johansson, 2019]

Definition (Ball interval)

A *ball interval* $[m \pm r]$ is defined as the set of real numbers x such that $x \in [m - r, m + r]$ where m denotes the *midpoint* of the ball interval and r its *radius*.

Computation of the joint stops

- Compute $\mathrm{IGM}(\mathcal{W}^\star) \triangleq \mathcal{Q}^\star$ and set the *joint stops* $\mathcal{Q}_0^\star$
- Interval analysis $\longrightarrow$ *Ball arithmetic* [Hoeven, 2010, Johansson, 2019]

Definition (Ball interval)

A *ball interval* $[m \pm r]$ is defined as the set of real numbers x such that $x \in [m - r, m + r]$ where m denotes the *midpoint* of the ball interval and r its *radius*.

- Implemented in Maple (v. $\geq$ 2022) using `arb` library with the `RealBox(`m`,`r`)` function

Computation of the joint stops

- Compute $\mathrm{IGM}(\mathcal{W}^\star) \triangleq \mathcal{Q}^\star$ and set the *joint stops* $\mathcal{Q}_0^\star$
- Interval analysis $\longrightarrow$ *Ball arithmetic* [Hoeven, 2010, Johansson, 2019]

Definition (Ball interval)

A *ball interval* $[m \pm r]$ is defined as the set of real numbers x such that $x \in [m - r, m + r]$ where m denotes the *midpoint* of the ball interval and r its *radius*.

- Implemented in Maple (v. ≥ 2022) using `arb` library with the `RealBox(`m`,`r`)` function
- Leaf of solution of interest:

$$\boldsymbol{\chi}_0 = \boldsymbol{o}_0 = \begin{bmatrix} 0 & 0 & 0 \end{bmatrix}^\intercal \xleftrightarrow{(+++)} \begin{cases} \boldsymbol{\theta}_0 = \begin{bmatrix} \pi/2 & \pi/2 & \pi/2 \end{bmatrix}^\intercal \\ \boldsymbol{j}_0 = \begin{bmatrix} 1 & 1 & 1 \end{bmatrix}^\intercal \end{cases} \tag{2}$$

- Considering the invariance w.r.t. $\chi_3 \equiv o_3 = 0$: paving $\mathcal{W}^\star(o_3 = 0)$ in the (o_1, o_2)-plan

Certification of the FGM (Direct Kinematics)

Theorem (Kantorovich [Kantorovich, 1948, Merlet, 2006])

Let $\boldsymbol{f} : \mathcal{D} \subseteq \mathbb{R}^n \to \mathbb{R}^n$ *a function of class* C^2*. Let* $\boldsymbol{x}_0$ *be a point and* $\overline{\boldsymbol{U}}\left(\boldsymbol{x}_0\right)$ *its neighborhood defined by* $\overline{\boldsymbol{U}}\left(\boldsymbol{x}_0\right) \triangleq \{\boldsymbol{x} \in \mathcal{D} \text{ s.t. } \|\boldsymbol{x} - \boldsymbol{x}_0\|_\infty \leq 2B_0\}$*. Let* $\boldsymbol{J}_0 \triangleq \boldsymbol{J}\left(\boldsymbol{x}_0\right) = \partial \boldsymbol{f} / \partial \boldsymbol{x}|_{\boldsymbol{x}=\boldsymbol{x}_0}$ *be an invertible jacobian matrix. If there exists three real constants* A_0*,* B_0 *and* C *such that:*

1. $\left\|\boldsymbol{J}_0^{-1}\right\|_\infty \leq A_0$
2. $\left\|\boldsymbol{J}_0^{-1} \boldsymbol{f}\left(\boldsymbol{x}_0\right)\right\|_\infty \leq B_0$
3. $\forall i \in [\![1, n]\!], \forall j \in [\![1, n]\!]$ *and* $\boldsymbol{x} \in \overline{\boldsymbol{U}}\left(\boldsymbol{x}_0\right)$, $\displaystyle\sum_{k=1}^{n} \left| \frac{\partial^2 f_i(\boldsymbol{x})}{\partial x_j \partial x_k} \right| \leq C$
4. $2nA_0B_0C \leq 1$

then there is a unique solution of $\boldsymbol{f}(\boldsymbol{x}) = \boldsymbol{0}$ *in* $\overline{\boldsymbol{U}}\left(\boldsymbol{x}_0\right)$ *and the (real) Newton iterative scheme* $\boldsymbol{x}_{k+1} = \boldsymbol{x}_k - \boldsymbol{J}^{-1}\left(\boldsymbol{x}_k\right) \boldsymbol{f}\left(\boldsymbol{x}_k\right)$ *with the initial estimate* $\boldsymbol{x}_0$ *quadratically converges towards this unique solution.*

Implementation of Path Tracking

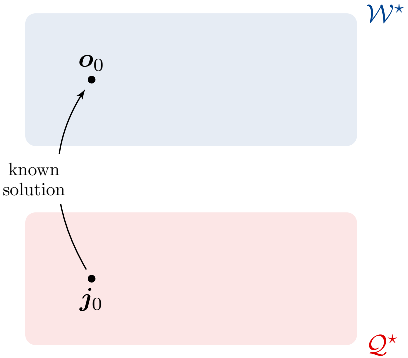

Figure: Path Tracking using the Kantorovich unicity operator

Implementation of Path Tracking

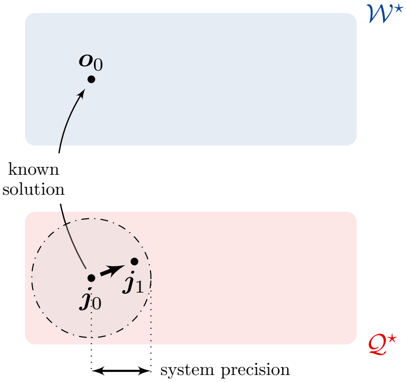

Figure: Path Tracking using the Kantorovich unicity operator

Implementation of Path Tracking

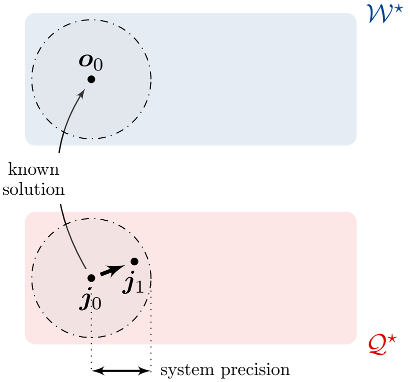

Figure: Path Tracking using the Kantorovich unicity operator

- A_0, B_0 and C are computed using *multiple-precision* arithmetic.

Implementation of Path Tracking

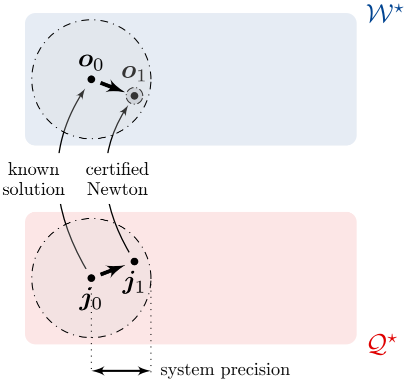

Figure: Path Tracking using the Kantorovich unicity operator

- A_0, B_0 and C are computed using *multiple-precision* arithmetic.
- Solutions $\boldsymbol{o}_k$ (returned by the Newton scheme) are isolated with *intervals*.

Implementation of Path Tracking

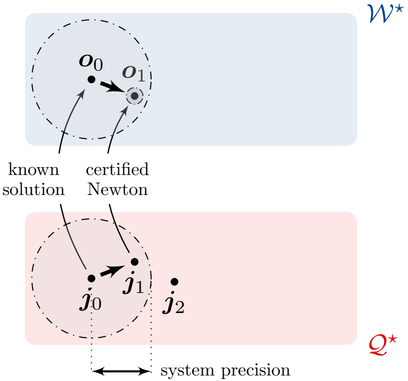

Figure: Path Tracking using the Kantorovich unicity operator

- A_0, B_0 and C are computed using *multiple-precision* arithmetic.
- Solutions $\boldsymbol{o}_k$ (returned by the Newton scheme) are isolated with *intervals*.

Implementation of Path Tracking

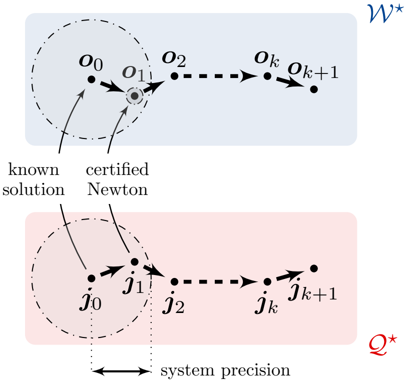

Figure: Path Tracking using the Kantorovich unicity operator

- A_0, B_0 and C are computed using *multiple-precision* arithmetic.
- Solutions $\boldsymbol{o}_k$ (returned by the Newton scheme) are isolated with *intervals*.

Conclusion

Conclusion: what has been done?

Problem

Certify a (spherical parallel) mechanism ***given specifications in*** $\mathcal{W}^\star$.

Certifying its Inverse Kinematics (IGM)

- *Exact symbolic* methods: *Discriminant Variety* of the IGM
- Computation of joints stops using *ball arithmetic*: $\mathcal{Q}^\star = \mathrm{IGM}(\mathcal{W}^\star)$

Certifying its Direct Kinematics (FGM)

- Use of a *semi-numerical* approach: certified *path tracking* in orientation

Maple

The End. Thank you!

Appendix

Bai, S. (2010).
Optimum design of spherical parallel manipulators for a prescribed workspace.
Mechanism and Machine Theory, 45(2):200–211.

Chablat, D., Moroz, G., Rouillier, F., and Wenger, P. (2020).
Using Maple to analyse parallel robots.
In Gerhard, J. and Kotsireas, I., editors, *Maple in Mathematics Education and Research*, Maple in Mathematics Education and Research, pages 50–64. Springer, Cham.

Gosselin, C. and Hamel, J.-F. (1994).
The agile eye: a high-performance three-degree-of-freedom camera-orienting device.
In *Proceedings of the 1994 IEEE International Conference on Robotics and Automation*, pages 781–786 vol.1.

Hoeven, J. (2010).
Ball arithmetic.

References II

Johansson, F. (2019).
Ball arithmetic as a tool in computer algebra.
In *MC*.

Kantorovich, L. V. (1948).
On Newton's method for functional equations.
In *Dokl. Akad. Nauk SSSR*, volume 59, pages 1237–1240.

Lazard, D. and Rouillier, F. (2007).
Solving parametric polynomial systems.
Journal of Symbolic Computation, 42(6):636–667.

Merlet, J.-P. (2006).
Parallel Robots (Second Edition).
Springer.

Shintemirov, A., Niyetkaliyev, A., and Rubagotti, M. (2015).
Numerical optimal control of a spherical parallel manipulator based on unique kinematic solutions.
IEEE/ASME Transactions on Mechatronics, 21:1–1.

References III

Tursynbek, I., Niyetkaliye, A., and Shintemirov, A. (2019).
Computation of unique kinematic solutions of a spherical parallel manipulator with coaxial input shafts.
In *2019 IEEE 15th International Conference on Automation Science and Engineering (CASE)*, pages 1524–1531.

Tursynbek, I. and Shintemirov, A. (2020).
Infinite torsional motion generation of a spherical parallel manipulator with coaxial input axes.
2020 IEEE/ASME International Conference on Advanced Intelligent Mechatronics (AIM), pages 1780–1785.

IGM Certification: Further information

Uncertainties on fabrication parameters

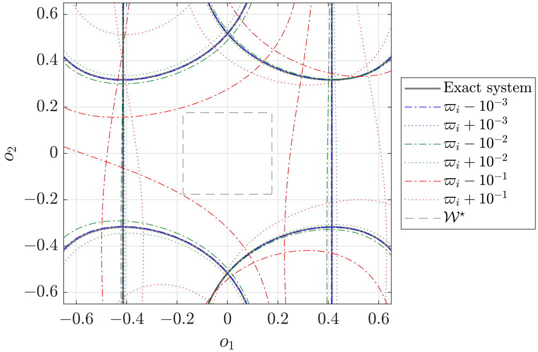

Figure: Type-1 singularity loci of the SPM in the orientation space considering uncertainties on the fabrication parameters $\boldsymbol{\varpi} \triangleq \begin{bmatrix} \alpha_1 & \alpha_2 & \beta_2 & \eta_1 & \eta_2 & \eta_3 \end{bmatrix}^\mathsf{T}$

- Considering $\beta_1 = 0$ (coaxiality), maximum tolerance on fabrication parameters of 10^{-1} rad

Details on the computation of the joint stops

Joint i	$\min(j_i)$	$\max(j_i)$	Joint stops	$\max(r(j_i))$	$\min(\Delta(p_i, j_i))$
1	0.6693723886	1.525710784	$\theta_1 \in [67°, 114°]$	0.05831109206017	3.149730917
2	0.6089969554	2.127382005	$\theta_2 \in [62°, 130°]$	0.18036268138497	10.08465368
3	0.4729818360	1.702299683	$\theta_3 \in [50°, 120°]$	0.15685467160577	10.01625750

Table: Extrema joint values obtained after the computation of the IGM of $\mathcal{W}^\star$ ($o_3 = 0$)

Details on the computation of the joint stops

Joint i	$\min(j_i)$	$\max(j_i)$	Joint stops	$\max(r(j_i))$	$\min(\Delta(p_i, j_i))$
1	0.6693723886	1.525710784	$\theta_1 \in [67°, 114°]$	0.05831109206017	3.149730917
2	0.6089969554	2.127382005	$\theta_2 \in [62°, 130°]$	0.18036268138497	10.08465368
3	0.4729818360	1.702299683	$\theta_3 \in [50°, 120°]$	0.15685467160577	10.01625750

Table: Extrema joint values obtained after the computation of the IGM of $\mathcal{W}^\star$ ($o_3 = 0$)

- Joint stops:

$$\mathcal{Q}_0^\star \triangleq \left\{ (\theta_1, \theta_2, \theta_3) \in \mathbb{R}^3 \;\middle|\; \begin{array}{l} 67° \leq \theta_1 - \chi_3 \leq 114° \\ 62° \leq \theta_2 - \chi_3 \leq 130°, \quad \forall\, \chi_3 \in \mathbb{R} \\ 50° \leq \theta_3 - \chi_3 \leq 120° \end{array} \right\} \tag{3}$$

- Image of $\mathcal{W}^\star$ through the IGM:

$$\mathcal{Q}^\star \triangleq \left\{ \boldsymbol{\theta} = \begin{bmatrix} \theta_1 & \theta_2 & \theta_3 \end{bmatrix}^\mathsf{T} \in \mathbb{R}^3 \;\middle|\; \boldsymbol{\theta} \in \mathcal{Q}_0^\star \text{ and } \mathrm{FGM}(\boldsymbol{\theta}) \in \mathcal{W}^\star \right\} \tag{4}$$